Research Square

Preprints are preliminary reports that have not undergone peer review. They should not be considered conclusive, used to inform clinical practice, or referenced by the media as validated information.

Plasma Radio–Metabolite Analysis of PET Tracers for Dynamic PET Imaging: TLC and Autoradiography

Fiona Li
The University of Western Ontario https://orcid.org/0000-0002-2423-6953
Justin W Hicks
Lawson Health Research Institute
Lihai Yu
Lawson Health Research Institute
Lise Desjardin
Lawson Health Research Institute
Laura Morrison
Lawson Health Research Institute
Jennifer Hadway
Lawson Health Research Institute
Ting-Yim Lee (tlee@robarts.ca)
https://orcid.org/0000-0001-7605-9752

Original research

Keywords: [18F]FEPPA, [18F]FAZA, Radio-metabolite Correction, Thin Layer Chromatography (TLC), Dynamic PET, Autoradiography

Posted Date: June 19th, 2020

DOI: https://doi.org/10.21203/rs.3.rs-35592/v1

License: This work is licensed under a Creative Commons Attribution 4.0 International License. Read Full License

Version of Record: A version of this preprint was published on November 23rd, 2020. See the published version at https://doi.org/10.1186/s13550-020-00705-2.

Plasma radio–metabolite analysis of PET tracers for dynamic PET imaging: TLC and autoradiography

[1,2,3]Fiona Li, [1,2]Justin W. Hicks, [2]Lihai Yu, [2]Lise Desjardin, [2]Laura Morrison, [2,3]Jennifer Hadway and [1,2,3]Ting-Yim Lee

[1]Department of Medical Biophysics, The University of Western University, London, Ontario, Canada

[2]Lawson Health Research Institute, London, Ontario, Canada

[3]Robarts Research Institute, London, Ontario, Canada

Background

In molecular imaging with dynamic PET, the binding and dissociation of a targeted tracer is characterized by kinetics modeling which requires the arterial concentration of the tracer to be measured accurately. Metabolism of the radiolabeled parent tracer in the body due to hydrolysis, methylation and other biochemical processes, results in the production and accumulation of different metabolites in blood which can be labeled with the same PET radionuclide as the parent. Since these radio-metabolites cannot be distinguished by PET scanning from the parent tracer, their contribution to the arterial concentration curve has to be removed for the accurate estimation of kinetic parameters from kinetic analysis of dynamic PET. High performance liquid chromatography has been used to separate and measure radio-metabolites in blood plasma, however, the method is labor intensive and remains a challenge to implement for each individual patient. The purpose of this study is to develop an alternate technique based on thin layer chromatography (TLC) and a sensitive commercial autoradiography system (Beaver, Ai4R, Nantes, France) to measure radio-metabolites in blood plasma of two targeted tracers □ [^{18}F]FAZA and [^{18}F]FEPPA , for imaging hypoxia and inflammation respectively.

Results

Radioactivity as low as 17Bq in 2µL of plasma can be detected on the TLC plate using autoradiography. Peaks corresponding to the parent tracer and radio-metabolites could be distinguished in the line profile through each sample (n=8) in the autoradiographic image. Significant inter-subject and intra-subject variability in radio-metabolites production could be observed with both tracers. For [^{18}F]FEPPA, 50% of plasma activity was from radio-metabolites as early as 5 min post injection while for [^{18}F]FAZA, significant metabolites did not appear until 50 min post. Simulation study investigating the effect of radio-metabolite in the estimation of kinetic parameters indicated that 32-400% parameter error can result without radio-metabolites correction.

Conclusion

TLC coupled with autoradiography is a good alternative to high performance liquid chromatography for radio-metabolite correction. The advantages of requiring only small blood samples (~ 100 □L) and of analyzing multiple samples simultaneously, make the method suitable for individual dynamic PET studies.

Keywords: [^{18}F]FEPPA, [^{18}F]FAZA, Radio-metabolite Correction, Thin Layer Chromatography (TLC), Dynamic PET, Autoradiography

1. Background

To derive molecular/metabolic information from dynamic positron emission tomography (PET), a kinetic analysis of the radiolabeled tracer is required. Obtaining the time concentration curve of the radiotracer in blood plasma, the arterial input function (AIF), is crucial to accurately portray the pathophysiology. One frequently used method is to sample arterial blood serially and use a radiation detector to measure the activity in the blood samples. The detector only detects the annihilation photons from the decaying positron-emitting isotope and cannot distinguish whether the radionuclide remains attached to the parent tracer or its metabolites (1). AIF can also be image derived obtained by measuring the activity in an arterial region in dynamic PET. Regardless of the method, measuring the activity in blood could overestimate the AIF because of the metabolite activity. Without correcting for the metabolite activity, results from kinetic analysis based on the overestimated AIF would be erroneous.

The metabolites can be separated from the parent tracer using chromatographic technique like thin layer chromatography (TLC), solid–phase extraction (SPE), or high performance liquid chromatography (HPLC) (2,3). A rapid separation method, SPE techniques require a high amount of manual manipulation, which may pose a safety hazard from routine use. They can also be used to purify samples before they are submitted to HPLC for further analysis (4). HPLC is widely used in analytical chemistry and pharmaceutical industry and research to determine the purity of samples. It has high resolution between metabolites and parent tracer with high sensitivity in radioactivity detection due to the use of a scintillation detector coupled with a photo-multiplier tube (5). However, as a serial analyzer, HPLC can only analyze one sample at a time which can take up to 20 min for each sample. These instruments rely on finely tuned pumps, sensitive detectors, and various separation media. This results in high initial purchasing and upkeep costs. Preparing plasma samples for HPLC analysis can be labor intensive and exposes personnel to additional ionizing radiation. Finally, HPLC separation is susceptible to impurities in the solvent mobile phases (1).

An economical alternative to HPLC is TLC which is a simpler version of HPLC. It is not susceptible to impurities and multiple samples can be analyzed at the same time. The major drawbacks are that TLC suffers from poorer analyte resolution and requires a very sensitive detector to detect analytes at low concentration on the TLC plate. Different techniques have been developed in the past for radio-TLC. Earlier techniques include the zonal analysis (6) and autoradiography technique where the TLC plate is directly exposed to x-ray film (7). Later, radio-scanners were developed that measured radioactivity at 1 – 2 mm steps. These techniques have poor analyte

101 resolution (albeit from the intrinsic TLC characteristics), low sensitivity (MBq/mL range), and usually require long
102 exposure time from hours to months for low activity samples and are prone to error (5,7). Therefore, our objective
103 was to explore a different detection system with improved sensitivity and time efficiency for radio-TLC.

104 2. **Methods**

105 2.1. **Beaver autoradiography system**

106 Beaver autoradiography (ai4r, France) is a multimodality real time digital autoradiography system that can
107 image beta and alpha particles (8). The detector is based on the principle of micro pattern gaseous (Ne + 10% CO_2)
108 detector (MPGD). The one we used was designed for imaging large samples with high spatial resolution of 50µm and
109 sensitivity of $5x10^{-4}$ $cpm.mm^{-2}$ (9). The detector is comprised of two drift zones alternating with two amplification
110 zones separated by nickel micromeshes (Figure 1). The special feature of the drift zone is the low electric field
111 (1kV/cm) that guides the electrons from the site of ionization by beta particles from radionuclide decay into the
112 amplification zone (10). Electrons are multiplied by avalanche effect in the amplification zone due to kinetic energy
113 imparted by the high electric field. The amplification zones are shallow in depth (50□m) to limit the spread of
114 electron avalanche (cloud) and hence improve spatial resolution (11). The TLC plate is used as the cathode of the
115 detector and serves as the back end of the first drift zone to prevent back flux of electrons. The electron cloud exiting
116 the second amplification zone is captured by the pixelated reading anode.

117 **2.2. Animal protocol**

118 All experimental procedures were approved by and performed in accordance with guidelines from
119 institutional animal ethics committee. Five farm pigs were procured from a farm nearby and two athymic Rowett
120 Nude (RNU) rats were purchased from Charles River (Saint Constant, Quebec, Canada). The C57BL/10J mouse used
121 in optimization of [^{18}F]FEPPA mobile phase was purchased from Jackson Laboratory (Maine, USA). The animals were
122 under no dietary restriction with free food access before each experiment. Pigs were first anesthetized with Telazole
123 intramuscular injection (1 mL/kg) while rats and mouse by masking with 5% isoflurane, and maintained using
124 isoflurane at 2-3% balanced oxygen and medical air. Pigs (33.7 ± 9.33 kg) were used for [^{18}F]FEPPA (21.9 ± 6.34
125 MBq/kg) analysis. [^{18}F]FEPPA rats (309.75 ± 29.64 g) were used for [^{18}F]FAZA (49.54 ± 9.39 MBq/kg) analysis. The
126 tracers were manufactured at the cyclotron/radiochemistry facility of our institution following published procedures
127 (12,13). Blood samples were drawn at 8 time points post tracer injection (p.i.) – 5, 10, 15, 20, 30, 40, 50 and 60 min.

128 Each rat underwent two blood draws, two weeks apart, to make up a total of 4 sets of rat blood samples. For rats,
129 blood (0.2 mL) was drawn for each sample from a tail vein using heparinized syringe into plasma separator tube. Due
130 to the larger total blood volume of pigs, 2mL of blood was drawn for each sample from a cephalic vein into EDTA
131 coated tubes.

132 **2.3. Blood preparation for metabolite analysis**

133 The blood samples were immediately placed on ice to prevent further catabolism. Within 1-2 min after the
134 last sample was taken, all samples were centrifuged at 1,000G in Sero-fuge II centrifuge (Clay-Adams Company, Inc.)
135 for 5 minutes. The supernatant plasma was aspirated for radio-metabolite analysis.

136 **2.4. Thin Layer Chromatography (TLC) preparation**

137 Silica coated TLC plates with F_{254} fluorescent indicator were purchased from MilliporeSigma. Each plate was
138 scored to a height of 9 cm to fit the 13x9 cm holder of the Beaver TLC detector. Blood plasma (2 µL) from each blood
139 sample was spotted 1 cm from the bottom of the plate with a micropipette. For optimal use of each imaging session
140 with the TLC detector, two 5 cm wide plates were used. Five samples including one parent tracer reference (0.11 –
141 0.30 MBq in 3 – 5 mL of isotonic saline) can be spotted on each plate. The plate was air dried after spotting then
142 immersed into the mobile phase in a beaker, making sure the solution was less than 5 mm high. The beaker was
143 then covered with parafilm wax paper. The TLC plate developed for approximately 15 minutes until the solvent
144 (mobile phase) front was roughly 1cm from the top of the plate. The plate was then removed, air dried, and imaged
145 with the autoradiographic detector for 4 h.

146 **2.5. Optimization of the mobile phase**

147 Using different volume fractions of ethyl acetate, methanol, and hexane, the mobile phase was optimized
148 for each tracer. The solution that allowed the least polar analyte to migrate furthest away from the spotting baseline
149 as well as giving a good separation of the metabolites from the unmodified tracer in the autoradiography image was
150 selected as optimized solution. Due to poor analyte resolution with TLC, the plasma metabolites did not appear as
151 discrete spots. [^{18}F]FEPPA and [^{18}F]FAZA were optimized with blood from a mouse and a human volunteer
152 respectively, drawn at 90 min and 60 min p.i. respectively. In this study, with the optimized mobile phase (solvent),
153 the parent tracer was always closest to the solvent front after the TLC plate was developed.

2.6. Image analysis

Autoradiography images were analyzed with Analyze 12.0 (Analyze Software System). Line profiles were generated by summing the detected counts in a 7 mm segment centered on the sample "track" at 10 mm intervals.

For line profiles where the adjacent metabolite peak overlapped with the parent tracer peak, the area underneath the latter was estimated with a custom developed program using MATLAB (The MathWorks, Inc.). These line profiles were fitted with two Gaussian functions. The parent tracer peak area was determined as the area of the fitted Gaussian between the limits of □ □ 1.96 □, where □ is the mean and □ is the standard deviation. For spots where the adjacent metabolite peak did not overlap with the parent tracer peak, the latter was fitted with a Gaussian function and the parent tracer peak area was similarly determined as for the case of overlap.

The fraction of the parent tracer was calculated using the formula:

$$fraction = \frac{Area\ under\ native\ tracer}{Total\ area\ under\ line\ profile}$$

Each estimated parent tracer fraction for different times p.i. was compared to published literature values for validation.

2.7. Effect of radio-metabolites on kinetic parameter estimation

The kinetic parameters associated with the tracer uptake are obtained by deconvolving the AIF of the parent tracer from the measured tissue concentration curve or tissue time activity curve (TAC). A simulation study was performed to observe the effect of blood plasma radio-metabolites in the estimation of kinetic parameters. For simulating the tissue TAC, our in-house flow modified two compartment (F2TC) model (14) that models the bi-directional permeation of the endothelial barrier during the transit time of the tracer through blood vessels, was utilized. The flow scaled impulse residue function ($IRF_F(t)$) for the model is expressed as:

$$IRF_F(t) = \begin{cases} F & 0 \le t < W \\ Ge^{-\alpha(t-W)} + He^{-\beta(t-W)} & t \ge W \end{cases}$$

175 where F is the blood flow, W is the mean transit time through blood vessels and G, H, α and β are the fitting
176 parameters obtained by iteratively fitting tissue TAC with non-linear 'interior point' optimization technique. The
177 model's explicit parameters can be calculated from the fitting parameters as follows:

178 $$K_1 = G + H;\ \ k_2 = \frac{G\alpha + H\beta}{G + H}$$

179 $$k_3 = \frac{GH(\alpha - \beta)^2}{(G + H)(G\alpha + H\beta)};\ \ k_4 = \frac{(G + H)\alpha\beta}{(G\alpha + H\beta)} = \frac{\alpha\beta}{k_2}$$

180 The explicit parameters are the influx (K_1) and efflux (k_2) rate constant of tracer through the blood tissue barrier and
181 k_3 and k_4 are the binding and disassociation rate constant of the parent tracer to and from the target respectively.

182 The measured AIF with metabolite contamination, AIF_m was simulated using Feng's model (15,16):

183 $$AIF_m(t) = [A_1(t - t_0)^\alpha - A_2 - A_3]e^{-\lambda_1(t-t_0)} + A_2 e^{-\lambda_2(t-t_0)} + A_3 e^{-\lambda_3(t-t_0)}$$

184 where $A_1 = 800, \alpha = 1.0,\ A_2 = 20,\ A_3 = 20,\ \lambda_1 = 4\ min^{-1}, \lambda_2 = 0.015\ min^{-1},\ \lambda_3 = 0.15\ min^{-1}, t_0 =$
185 $0.15\ min$

186 AIF_m was simulated at 0.5 s and corrected for radio-metabolite by multiplying with the fraction of parent [^{18}F]FEPPA
187 measured in §3.4:

188 $$AIF_c = AIF_m * fraction$$

189 The corrected AIF_C was used to simulated tissue TAC at 0.5 s with ten sets of parameters (Table 1) from patients with
190 high grade glioma (17). All the curves were frame averaged according to the following frame schedule: 10 @ 10 s, 5
191 @ 20 s, 4 @ 40 s, 4 @ 60 s, 11 @ 180 s and 1@ 120 s (total 45 min). The two sets of kinetic parameters estimated
192 by deconvolving AIF_m and AIF_c from simulated tissue TACs were compared. The difference of the parameters
193 estimated with and without metabolite correction was tested for statistical significance using non-parametric test
194 □ either Wilcoxon signed rank or sign test depending on whether the distribution of the differences was symmetric
195 or non-symmetric, respectively. P<0.05 was declared significant with Bonferroni correction for multiple comparison
196 with 8 parameters ($K_1, k_i\ (i = 2,3,4), V_p, DV, W, K_i$).

Table 1 Ten parameter sets used for simulating the effect of radio-metabolite correction in blood plasma

SET#	K_1 (mL□min^{-1}□g^{-1})	k_2 (min^{-1})	k_3 (min^{-1})	k_4 (min^{-1})	F (mL□min^{-1}□g^{-1})	W (s)	V_p (mL□g^{-1})	DV (mL.g^{-1})
1	0.0930	0.5920	0.1840	0.0410	0.37	7	0.043	0.8621
2	0.1370	0.3310	0.2300	0.0700	0.27	7	0.032	1.7738
3	0.0740	0.3440	0.1520	0.0370	0.10	10	0.016	1.0988
4	0.0720	0.4580	0.2880	0.0770	0.29	10	0.048	0.7452
5	0.2220	0.4720	0.1900	0.0870	0.44	5	0.037	1.4975
6	0.1940	0.3280	0.2830	0.1720	0.26	15	0.065	1.5646
7	0.0960	1.0000	0.3060	0.0670	0.38	8	0.051	0.5344
8	0.1010	0.5180	0.3510	0.0750	0.20	10	0.034	1.1075
9	0.4790	1.0000	0.2210	0.1370	0.64	10	0.106	1.2517
10	0.2180	0.4980	0.4480	0.0840	0.87	15	0.218	2.7724

3. Results

3.1. Optimization of the mobile phase

The separation of radio-metabolites in blood plasma with different mixtures of methanol, hexane and ethyl acetate for both tracers is shown in Figure 2. The optimized mobile phase for [^{18}F]FEPPA and [^{18}F]FAZA were 8% methanol and 10% hexane in ethyl acetate (v/v; fourth solution) and 7% methanol in ethyl acetate (v/v; third solution) respectively.

3.2. Autoradiography

Figure 3 shows the autoradiographic images obtained from TLC plasma metabolite analysis of [^{18}F]FAZA (rat) or [^{18}F]FEPPA (pig), respectively. Each image showed two TLC plates with the parent tracer in normal saline as reference on each, as well as plasma obtained at different times p.i.. Since the reference parent tracer spot moved the furthest from the spotting baseline, it was the least polar analyte. The spots with similar retention factors (R_f) to the reference spots were the fractions of the parent tracer in plasma at different times p.i.. For [^{18}F]FAZA on the left, the reference spots' R_f was 0.66 ± 0.01 . Most of the activity was from the parent tracer while that at the spotting line could be from the more polar radio-metabolites. Significant conversion of tracer to radio-metabolite was observed from 50 min p.i.. For [^{18}F]FEPPA on the right, the reference spots' R_f was 0.54 ± 0. Radio-metabolites were

observed as early as 5 min p.i. as indicated by activity directly below the reference R_f as well as activity along the spotting line. At 1 h p.i., the parent tracer spot almost disappeared as there was almost complete conversion into metabolites observed as activity all along the track.

3.3. Line profile

Figure 4 shows the line profiles of selected [^{18}F]FEPPA spots reference, 5 min and 1 h p.i. in the right image of Figure 3. For the reference, a well-defined peak was observed due to high signal to noise ratio. At 5 min p.i., three prominent peaks were discernible. The peak on the furthest right was the parent [^{18}F]FEPPA, the peak for the least polar radio–metabolite was close to the parent tracer. The most polar radio-metabolite was located close to the spotting baseline. At 1 h p.i., the parent [^{18}F]FEPPA peak was not identifiable. A new peak corresponding to radio-metabolites of intermediate polarity was observed and the amount of the most polar radio-metabolite increased, as indicated by the area. Therefore, the parent [^{18}F]FEPPA was almost completely metabolized to radio-metabolites at 1 h p.i..

Table 2 Coefficient of variation of parent tracer fraction for [^{18}F]FEPPA and [^{18}F]FAZA

	5 min	**10 min**	**15 min**	**20 min**	**30 min**	**40 min**	**50 min**	**60 min**
[^{18}F]FEPPA	0.07	0.13	0.17	0.17	0.24	0.32	0.26	0.43
[^{18}F]FAZA	0.02	0.03	0.03	0.04	0.01	0.03	0.12	0.25

3.4. Fraction of parent tracer versus post-injection time

Figure 5 shows the fraction of parent [^{18}F]FAZA and [^{18}F]FEPPA in blood at different times post-injection. For [^{18}F]FAZA, the fraction of parent tracer remained relatively constant at 91% until 40 min p.i. The fraction then decreased to 62% and 40% at 50 and 60 min p.i., respectively. On the other hand, close to 50% of activity in blood was from [^{18}F]FEPPA metabolites as early as 5 min p.i. and the parent tracer fraction decreased to 19% at 1 hour p.i. Table 2 shows the coefficient of variation (CoV) of the parent tracer fraction arising from inter-subject variability. For [^{18}F]FEPPA, CoV ranged from 0.07 to 0.43 while [^{18}F]FAZA from 0.01 to 0.25.

Table 3 Median differences in parameters estimated from simulation study

Parameter	K_1 (mL□min^{-1}□g^{-1})	k_2 (min^{-1})	k_3 (min^{-1})	k_4 (min^{-1})	V_p (ml.g^{-1})	DV (ml.g^{-1})	W (min)
Median difference	-0.001	-0.118	0.105	-0.043	0.006	0.718	0.021
P	0.75	0.004	0.005	0.004	0.013	0.004	0.083
*** Bias (%)**	403	-32.0	51.0	-171	71.0	50.0	166

Median differences between parameters in table 1 estimated using AIF with and without metabolite correction. P value is estimated by non-parametric paired test. *Although the differences in the estimated parameters were not normally distributed, the percentage bias was used to approximate the expected error

3.5. Simulation study

Due to conversion of parent tracer to radio-metabolite, metabolite correction lowered the AIF as p.i. time increased (Figure 6(a)). When AIF_C was deconvolved from the tissue TACs, the parameters estimated were statistically different from those estimated by deconvolving AIF_m; errors greater than 32% were observed for all parameters (Table 3).

4. Discussion

In this study, we established an alternate method to HPLC to determine the fraction of radio-labeled parent tracer at different times p.i. based on inexpensive TLC and a sensitive beta detector. Fraction of unmetabolized [^{18}F]FAZA and [^{18}F]FEPPA in normal healthy rats and pigs (respectively) p.i. were measured and compared to literature values, if available. There were large variations in the rate of metabolite production with the same tracer (either [^{18}F]FAZA or [^{18}F]FEPPA) and between the two tracers in the same and different animals. CoV of parent tracer fraction in blood could be as high as 43%. Since the mobile phase optimization and the successful metabolite analyses were performed on different animal species as well as human subject, it showed that the mobile phase could be optimized in animals and transferred to human population. Furthermore, simulation study investigating the effect of radio-metabolite correction in measured arterial curve suggested that large error (30 – 400%) can result in the estimation of kinetic parameters if correction was not incorporated.

The acquired autoradiography images showed clear distinction between radio-metabolites and the parent tracer. The large signal difference between reference and plasma sample was due to 6.7 times difference in the

activity between the two. Reference [^{18}F]FEPPA (parent tracer in normal saline) was spotted with activity of 126 ± 17 Bq in 2 uL while plasma samples from pigs were lower in activity – at 5 min p.i. the activity was approximately 17 Bq in 2 uL. For our metabolite studies, either 15.2 ± 1.8 MBq (41□ 59MBq/kg) or 427 □ 1216 MBq (13 □ 27 MBq/kg) was administered for the rat ([^{18}F]FAZA) and pig ([^{18}F]FEPPA), respectively at the time of injection. These were lower than other published metabolite studies in mice where doses ranging from 20 – 30 MBq (1 GBq/kg) (18) to as high as 68 MBq (3.4 GBq/kg) (19) of tracer were administered due to the lower sensitivity of the radiation detector used. In our studies, even with >77 times less dose (normalized to body weight to account for the body mass of different species), peaks corresponding to the parent tracer could be distinguished from radio-metabolites. In the few cases where radio-metabolites overlapped with the parent tracer because of similar polarity and hence strength of adhesion to the silica media, the parent tracer peak could be adequately resolved by the curve fitting procedure discussed in §2.6. Taken the above results together, our method of combining TLC and the Beaver proprietary beta particle detector has the analyte resolution and sensitivity for blood metabolite determination for both [^{18}F]FAZA and [^{18}F]FEPPA in individual large (pig) or small (rodents) animals. Nevertheless, by comparing the [^{18}F]FEPPA dose used in our pig studies (13□27 MBq/kg) to the published patient dose (2.5 □ 6.2 MBq/kg (20–23)) the sensitivity of the detector has to be increased by at least 5 times for the method to be used for blood metabolite determination in individual patients.

From the [^{18}F]FEPPA results (Table 2), inter-subject variation was observed with more pronounced variability at later time points p.i. This supports our view that the current practice of using a population average in normal subjects to correct for metabolite contamination (24) is not optimal for kinetic analysis and there is a need to determine blood metabolite in individual studies. HPLC is the most commonly used method to measure metabolite fraction in blood. It is a serial analyzer; samples are analyzed one at a time. Because multiple timed samples must be analyzed, HPLC is both labor intensive and time consuming if it is used to construct the metabolite fraction curve over ~ 60 min for each individual study. This limitation has resulted in the use of population based (even cross species) blood metabolite fraction for individual studies with the assumption that the inter-subject (inter-species) variability in metabolite production is negligible. As our study and other studies showed (20,24,25), inter-subject variabilities do exist invalidating the above assumption. In contrast, with our method, multiple samples can

282 be analyzed together within one imaging session, the exact number of samples depends on the detector size.
283 Currently, we can analyze 8 samples but with a larger detector size, the number of samples can be increased to 12
284 or more making it feasible for individualized radio-metabolite analysis.

285 The effect of not correctly accounting for blood radio-metabolite was investigated with computer
286 simulation using a previously published kinetics model (14). For all parameter sets listed in Table 1, the fitting to the
287 simulated tissue time activity curve (TAC) failed when radio-metabolite contamination was not corrected for in the
288 arterial TAC. This failure led to large errors (30 – 400%) in parameter estimation and possible misinterpretation of
289 the tracer pharmacokinetics. For instance, distribution volume of [^{18}F]FAZA is related to the amount and activity of
290 nitroreductase present in hypoxic tissue (26) while that of [^{18}F]FEPPA is related to density and activity of translocator
291 protein (TSPO) found on the outer mitochondrial membrane (27), particularly within activated immune cells (28).

292 Our measured fractions of parent [^{18}F]FEPPA in blood over time p.i. agreed well with those obtained by
293 Rusjan et al. (20). On the other hand, measured fractions of parent [^{18}F]FAZA over time p.i. were not found in
294 literature. Studies of [^{18}F]FAZA by Verwer et al. showed that only 10% of the activity in blood was from metabolites
295 at 70 min p.i. (22) with the use of solid phase extraction and HPLC. Our study showed that significant metabolite
296 fraction (~ 10%) in blood started at 40 min and increased to 60% at 60 min p.i.. Jans et al (18) also used TLC to
297 estimate the metabolite fraction in blood and no metabolite was observed. However, there were two mitigating
298 factors with their experiments that could explain the difference in the measured metabolite fraction in blood. First,
299 it was not known whether the mobile phase used was optimized for the tracer; second, the detector used may not
300 be as sensitive as our one.

301 The time required for blood metabolite analysis using our method starting with the collected blood samples
302 (excluding the image processing time) comprised of: 5 min of centrifugation, 5 min for spotting samples on and
303 drying the TLC plate, and 15 minutes of TLC plate development for a total of 25 – 30 minutes. Technically, the solvent
304 front is required to move beyond the furthest point the samples or the parent tracer moved during development. In
305 our experiments, the parent tracer (either [^{18}F]FAZA or [^{18}F]FEPPA) which moved the furthest, moved approximately
306 4.5 cm while the solvent front moved over 7 cm. Therefore, the development time can be shortened to 10 min. The
307 autoradiograph image was acquired over 4 h in this study. However, one–hour acquisition was tested, the acquired

image showed good image quality (signal-to-noise ratio) as shown in the supplementary figure. Unlike HPLC where it occupies the operator's attention the entire time while the samples are analyzed, here the imaging (1 or 4 h) is completely operator independent.

In comparison, radio – HPLC takes approximately 10 min for each sample analyzed, not including sample preparation time. With multiple samples (say 8 samples as in this study), the total preparation time required could be over 80 min compared to 10 min with our method. Other comparative similarities and differences between our method and HPLC include the following. First, our method requires a smaller volume of plasma (2 □L) than HPLC. Sample volume required, ranging from 1 to 2000 µL, for HPLC depending on the size of the column (29). Second, both requires the mobile phase to be optimized for each tracer. Third, inexpensive TLC plates can be used for all tracers but can be used only once while different expensive HPLC columns may be required, one for each tracer but each column is reusable. Fourth, HPLC columns require regular washing to prevent clogging and to remove metabolites from previous runs which can cause residual memory issue (1,30); these issues do not arise with TLC because a new inexpensive plate is used for each metabolite analysis run and TLC is less prone to impurities present in the solvent. Fifth, HPLC has superior analyte resolution than TLC which avoids potential overlapping of the parent tracer peak with that of metabolites. However, this overlap of peaks can be resolved by Gaussian fitting as discussed in §2.6. Since the chemical identity of the radio-metabolites is not required for metabolite fraction correction, this simple correction method is sufficient for our purpose. Finally, the Beaver autoradiography system is marginally more expensive than an HPLC, however, it is a multipurpose system with tissue slice imaging capabilities able to detect both α and β particles. Taking all the above comparative advantages and disadvantages of our method and HPLC into consideration, we conclude that our method is more suited for individualized metabolite measurement in blood than HPLC. Note that independent of whether the AIF is measured with timed arterial blood sample or is image derived by measuring the activity in an arterial region in dynamic PET images, metabolite correction is required.

There are several limitations with our study. The measured blood metabolite fraction was not validated against the reference HPLC method. However, our [^{18}F]FEPPA results agreed with literature values measured with reverse phase HPLC (Figure 6(b)). The number of blood samples used for each tracer was small. Even with this small

number of animals, the inter-subject variability in metabolite fraction was prominent (Table 2) suggesting that this result could be the true *in vivo* situation and the importance to measure metabolite fraction for each individual subject. We investigated only two tracers, [^{18}F]FEPPA and [^{18}F]FAZA, as examples. Since analyte separation of TLC depends on the polarity of the tracer and its metabolites, for other tracers the mobile phase will have to be optimized. We have tested our method only with the ^{18}F radionuclide. Since other common PET radionuclides including ^{11}C, ^{13}N, ^{68}Ga and ^{89}Zr emit □$^{-}$ particles in their decay, our method would also work except, like the mobile phase, the limit of radioactivity detection must be determined for each radionuclide separately.

5. Conclusion

We were able to measure the fraction of parent radiolabeled tracer in blood after it was injected into the body using TLC and the Beaver autoradiography system. This fraction is required to correct the AIF obtained by measuring the activity in timed arterial blood samples or in arterial region in dynamic PET images. Without this correction, the AIF will be overestimated leading to errors in the kinetic analysis of dynamic PET. Although we used two specific tracers, [^{18}F]FAZA and [^{18}F]FEPPA, to develop the method, the system can be used for other tracers by optimizing the mobile phase for each of them. Due to its capability to analyze multiple (>8) blood samples at the same time with preparation time as short as 25 – 30 min, our method will enable individualize blood metabolite correction for kinetic analysis of dynamic PET.

357 **References**

358 1. Pawelke B. Metabolite analysis in positron emission tomography studies: Examples from food sciences.
359 Amino Acids. 2005;29(4 SPEC. ISS.):377–88.

360 2. Wang RF, Loc'h C, Mazière B. Determination of unchanged [18F]dopamine in human and nonhuman
361 primate plasma during positron emission tomography studies: A new solid-phase extraction method
362 comparable to radio-thin-layer chromatography analysis. J Chromatogr B Biomed Appl. 1997;693(2):265–
363 70.

364 3. Ma Y, Kiesewetter DO, Lang L, Der M, Huang B, Carson RE, et al. Determination of [18F]FCWAY, [18F]FP-
365 TZTP, and their metabolites in plasma using rapid and efficient liquid-liquid and solid phase extractions.
366 Nucl Med Biol. 2003;30(3):233–40.

367 4. Robards K, Haddad PR, Jackson PE. Principles and Practice of Modern Chromatographic Methods.
368 Academic Press; 1994. 1–32 p.

369 5. Takei M, Kida T, Suzuki K. Sensitive measurement of positron emitters eluted from HPLC. Appl Radiat Isot.
370 2001;55(2):229–34.

371 6. Snyder F, Cress E. Application of thin-layer chromatographic zonal 14C-Profile scans to the analysis of
372 urinary constituents derived from lipds. Clin Chem. 1968;14(6):529–34.

373 7. Marx AM, Kronberg H, Neuhoff V. Determination of the specific radioactivity of amino acids by a
374 combination of thin-layer chromatography and quantitative autoradiography. J Chromatogr.
375 1987;393(19):407–17.

376 8. Sardini P, Angileri A, Descostes M, Duval S, Oger T, Patrier P, et al. Quantitative autoradiography of alpha
377 particle emission in geo-materials using the Beaver^{TM} system. Nucl Instruments Methods Phys Res Sect A
378 Accel Spectrometers, Detect Assoc Equip. 2016;833:15–22.

379 9. Ai4r. BeaQuant. 2017. http://www.ai4r.com/real-time-autoradiography/product/. Accessed 31 Jan 2020.

380 10. Titov M. Perspectives of Micro-Pattern Gaseous Detector Technologies for Future Physics Projects. 2013;1–
381 14.

382 11. Donnard J, Arlicot N, Berny R, Carduner H, Leray P, Morteau E, et al. Advancements of labelled radio-
383 pharmaceutics imaging with the PIM-MPGD. J Instrum. 2009;4(11):1–9.

384 12. Wilson AA, Garcia A, Parkes J, McCormick P, Stephenson KA, Houle S, et al. Radiosynthesis and initial
385 evaluation of [18F]-FEPPA for PET imaging of peripheral benzodiazepine receptors. Nucl Med Biol.
386 2008;35(3):305–14.

387 13. Hayashi K, Furutsuka K, Takei M, Muto M, Nakao R, Aki H, et al. High-yield automated synthesis of
388 [18F]fluoroazomycin arabinoside ([18F]FAZA) for hypoxia-specific tumor imaging. Appl Radiat Isot
389 [Internet]. 2011;69(7):1007–13. Available from: http://dx.doi.org/10.1016/j.apradiso.2011.02.025

390 14. Yang DM, Palma D, Louie A, Malthaner R, Fortin D, Rodrigues G, et al. Assessment of tumour response after
391 stereotactic ablative radiation therapy for lung cancer: A prospective quantitative hybrid 18 F-
392 fluorodeoxyglucose-positron emission tomography and CT perfusion study. J Med Imaging Radiat Oncol.
393 2019;63(1):94–101.

394 15. Feng D, Huang S-C, Wang X. Models for computer simulation studies of input functions for tracer kinetic
395 modeling with positron emission tomography. Int J Biomed Comput. 1993;32(2):95–110.

396 16. Ben Bouallègue F, Vauchot F, Mariano-Goulart D. Comparative assessment of linear least-squares,
397 nonlinear least-squares, and Patlak graphical method for regional and local quantitative tracer kinetic
398 modeling in cerebral dynamic 18 F-FDG PET. Med Phys. 2019;46(3):1260–71.

399 17. Debus C, Afshar-Oromieh A, Floca R, Ingrisch M, Knoll M, Debus J, et al. Feasibility and robustness of
400 dynamic 18F-FET PET based tracer kinetic models applied to patients with recurrent high-grade glioma
401 prior to carbon ion irradiation. Sci Rep. 2018;8(1):1–17.

402 18. Jans HS, Yang XH, Brocks DR, Kumar P, Wuest M, Wiebe LI. Positron emission tomography (PET) and
403 pharmacokinetics: Classical blood sampling versus image-derived analysis of [18 F]FAZA and [18 F]FDG in

404 a murine tumor bearing model. J Pharm Pharm Sci. 2018;21(1S):32s-47s.

405 19. Vignal N, Cisternino S, Rizzo-Padoin N, San C, Hontonnou F, Gelé T, et al. [18F]FEPPA a TSPO radioligand:
406 Optimized radiosynthesis and evaluation as a PET radiotracer for brain inflammation in a peripheral LPS-
407 injected mouse model. Molecules. 2018;23(6).

408 20. Rusjan PM, Wilson AA, Bloomfield PM, Vitcu I, Meyer JH, Houle S, et al. Quantitation of translocator
409 protein binding in human brain with the novel radioligand 18 F-FEPPA and positron emission tomography. J
410 Cereb Blood Flow Metab. 2011;31(8):1807–16.

411 21. Mizrahi R, Rusjan PM, Vitcu I, Ng A, Wilson AA, Houle S, et al. Whole Body Biodistribution and Radiation
412 Dosimetry in Humans of a New PET Ligand, [18F]-FEPPA, to Image Translocator Protein (18 kDa). Mol
413 Imaging Biol. 2013;15(3):353–9.

414 22. Verwer EE, van Velden FHP, Bahce I, Yaqub M, Schuit RC, Windhorst AD, et al. Pharmacokinetic analysis of
415 [18F]FAZA in non-small cell lung cancer patients. Eur J Nucl Med Mol Imaging. 2013;40(10):1523–31.

416 23. Savi A, Incerti E, Fallanca F, BettinarDi V, Rossetti F, Monterisi C, et al. First evaluation of PET-based human
417 bioDistribution and dosimetry of 18F-FAZA, a tracer for imaging tumor hypoxia. J Nucl Med.
418 2017;58(8):1224–9.

419 24. Hinz R, Bhagwagar Z, Cowen PJ, Cunningham VJ, Grasby PM. Validation of a tracer kinetic model for the
420 quantification of 5-HT 2A receptors in human brain with [11C]MDL 100,907. J Cereb Blood Flow Metab.
421 2007;27(1):161–72.

422 25. Henriksen G, Spilker M, Sprenger T, Hauser A, Platzer S, Boecker H, et al. Gender dependent rate of
423 metabolism of the opiod receptor-PET ligand [18F]fluoroethydiprenorphine. Nuklearmedizin.
424 2006;45(5):197–200.

425 26. Nunn A, Linder K, Strauss HW. Nitroimidazoles and imaging hypoxia. Eur J Nucl Med. 1995;22(3):265–80.

426 27. Anholt R, Pedersen P, De Souza E, Snyder S. The peripheral-type benzodiazepine receptor: localization to
427 the mitochondrial outer membrane. J Biol Chem. 1986;261(2):576–83.

428 28. Veiga S, Carrero P, Perna O, Azcotta I, Garcia-Segura L. Translocator protein (18kDa) is involved in the
429 regulation of reactive gliosis. Glia. 2007;55:1425–36.

430 29. Silicycle. Ideal injection volume vs column dimension. 2019. https://www.silicycle.com/ca/faq/hplc/ideal-
431 injection-volume-vs-column-dimension Accessed 5 May 2020

432 30. Wilson ID. Thin-layer chromatography: A neglected technique. Ther Drug Monit. 1996;18(4):484–92.

433

434 **List of abbreviations**

435 AIF – Arterial input function

436 CoV – Coefficient of variation

437 DV – Distribution Volume

438 F – Blood flow

439 F2TC – Flow modified two compartment

440 HPLC – High performance liquid chromatography

441 IRF – Impulse residue function

442 K_1 – Influx rate constant

443 k_2 – Efflux rate constant

444 k_3 – Binding rate constant

445 k_4 – Disassociation rate constant

446 K_i – Net influx rate

447 MPGD – Micro pattern gaseous detector

448 p.i. – Post injection

PET – Positron emission tomography

R_f – retention factor

SPE – Solid –phase extraction

TAC – Time activity curve

TLC – Thin layer chromatography

V_p – Blood Volume

W – Mean transit time

Declarations

Ethics Approval: All animal studies were performed in accordance with guidelines from the institutional animal ethics board

Consent for publication: Not applicable

Availability of data and material: The datasets used and/or analysed during this study are available from the corresponding author on reasonable request.

Competing interests: The authors declare that they have no competing interests

Funding: This work was funded by a Quantitative Imaging Network grant from the Canadian Institutes for Health Research and National Institutes of Health.

Author's contribution: FL and T-Y L were involved in the design of the experiment in consultation with JWH. LD, JH and LM helped with the animal experiments. LY synthesized the radiotracers. FL performed the blood analysis, designed the simulation study, analyzed and interpreted the results, and wrote the manuscript with the assistance of T-Y Lee.

Acknowledgements:

The authors thank Dr. Jerome Donnard and Remy Sence of ai4r (Nantes, France) for helpful discussions. This work was supported in part by Lawson Health Research Institute and Robarts Research Institute

473

474 **Images**

Fig. 1 Schematic of Beaver Autoradiography

Working principle of Beaver MPGD for β- particles. (Adapted from *J Instrum. 2009;4:1-9 (11))*

475

Fig. 2 Autoradiographic image of mobile phase optimization for [^{18}F]FAZA and [^{18}F]FEPPA

Mobile phase optimization for (a) [^{18}F]FAZA and (b) [^{18}F]FEPPA in human and mouse blood respectively at 90 min and 60 min (respectively) post injection, using different fractions of methanol, ethyl acetate and hexane. For each tracer, five different mixtures were used. For [^{18}F]FAZA only blood samples were used while for [^{18}F]FEPPA each blood sample was paired with the native tracer in normal saline as the reference. The optimal mobile phase would spread the radio-metabolites along the entire lane and move the reference furthest from the spotting line. For [^{18}F]FEPPA the fourth solution from the left comprised of 8% methanol, 10% hexane and 82% ethyl acetate was optimal while for [^{18}F]FAZA, it was the third solution comprised of 7% methanol and 93% ethyl acetate.

476

Fig. 3 Autoradiographic image of plasma samples

Autoradiography image of plasma samples obtained from a rat injected with [^{18}F]FAZA (left) and from a pig injected with [^{18}F]FEPPA (right). 'Ref' is the reference spot on each TLC plate. The number above each line shows the time in min at which the blood sample was drawn post tracer injection. The direction of motion of the mobile phase (solvent) front from capillary action was from bottom to top. The radio-metabolites that did not move with mobile phase show up as faint 'spots' at the bottom along the spotting line.

477

Fig. 4 Line profile of [^{18}F]FEPPA

Line profile of [^{18}F]FEPPA reference, plasma from a pig obtained at 5 min and 1 h post tracer injection. The y-axis is detected counts and the x-axis is distance in mm. The corresponding autoradiography image is displayed above the profile. The direction of movement of the solvent front from capillary action was from left to right

478

Fig. 5 Fraction of parent tracer for [^{18}F]FAZA and [^{18}F]FEPPA

Native tracer fraction vs time post injection (p.i.) for (a) [^{18}F]FAZA and (b) [^{18}F]FEPPA. The dashed line in (b) was native tracer fraction from (18).The error bar corresponds to standard deviation for 5 pig blood samples ([^{18}F]FEPPA) and 4 rat blood samples ([^{18}F]FAZA)

479

Fig. 6 Simulation curves for estimating accuracy of kinetic parameter due radio-metabolite correction

Curves utilized for simulating the effect of radio-metabolite on kinetic parameter estimation in dynamic PET cases. (a) Arterial curve simulated with Feng's model for measured (not corrected, dashed line) and radio-metabolite corrected curve (solid line). (b) Tissue curve simulated with parameter set #6 (table 1, solid square) and fitted curves obtained with measured arterial curve (dashed line) and with radio-metabolite corrected arterial curve (solid line).

480

481 **Supplementary Figure**

482

Beaver image of blood plasma obtained from a rat injected with [^{18}F]FAZA. The SNR of image (a) acquire for 1 hour is acceptable with discernible spots for native tracer and radio-metabolites. (b) The same TLC image that is acquired for four hours immediately after (a) was acquired. The bright spot is the reference 'ref' native tracer followed by blood samples drawn at 30, 40, 50 and 60 minute post injection.

Figures

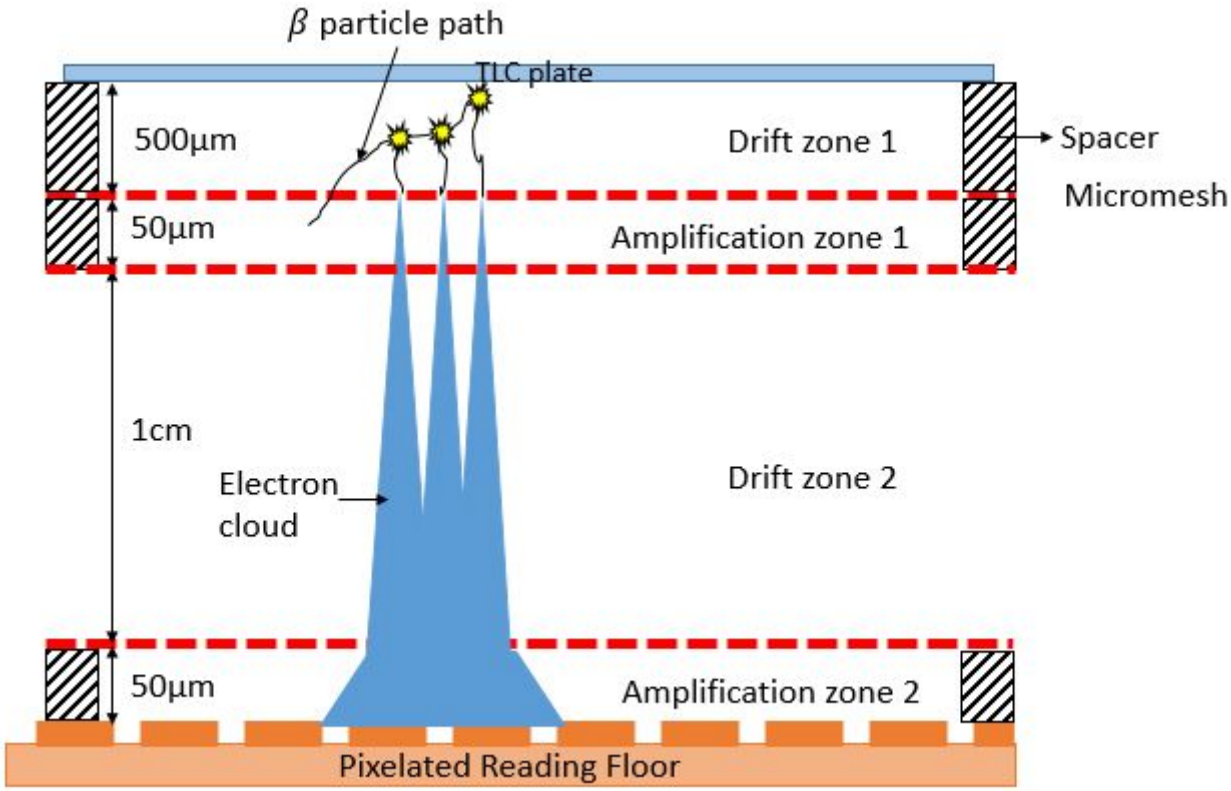

Figure 1

Schematic of Beaver Autoradiography Working principle of Beaver MPGD for β- particles. (Adapted from J Instrum. 2009;4:1-9 (11))

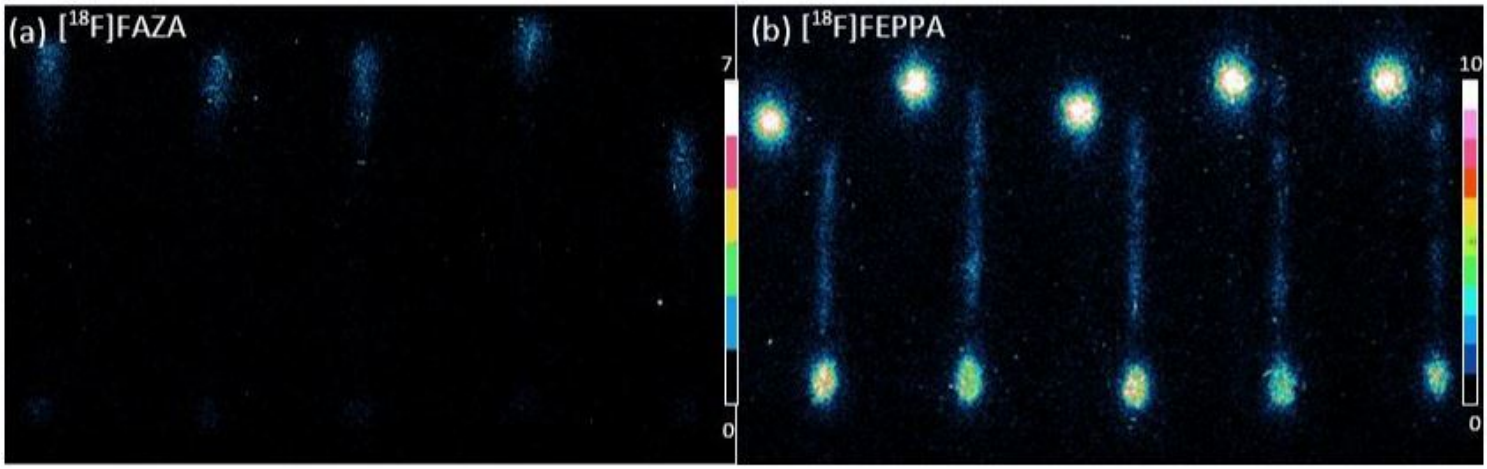

Figure 2

Autoradiographic image of mobile phase optimization for [18F]FAZA and [18F]FEPPA Mobile phase optimization for (a) [18F]FAZA and (b) [18F]FEPPA in human and mouse blood respectively at 90 min and 60 min (respectively) post injection, using different fractions of methanol, ethyl acetate and hexane. For

each tracer, five different mixtures were used. For [18F]FAZA only blood samples were used while for [18F]FEPPA each blood sample was paired with the native tracer in normal saline as the reference. The optimal mobile phase would spread the radio-metabolites along the entire lane and move the reference furthest from the spotting line. For [18F]FEPPA the fourth solution from the left comprised of 8% methanol, 10% hexane and 82% ethyl acetate was optimal while for [18F]FAZA, it was the third solution comprised of 7% methanol and 93% ethyl acetate.

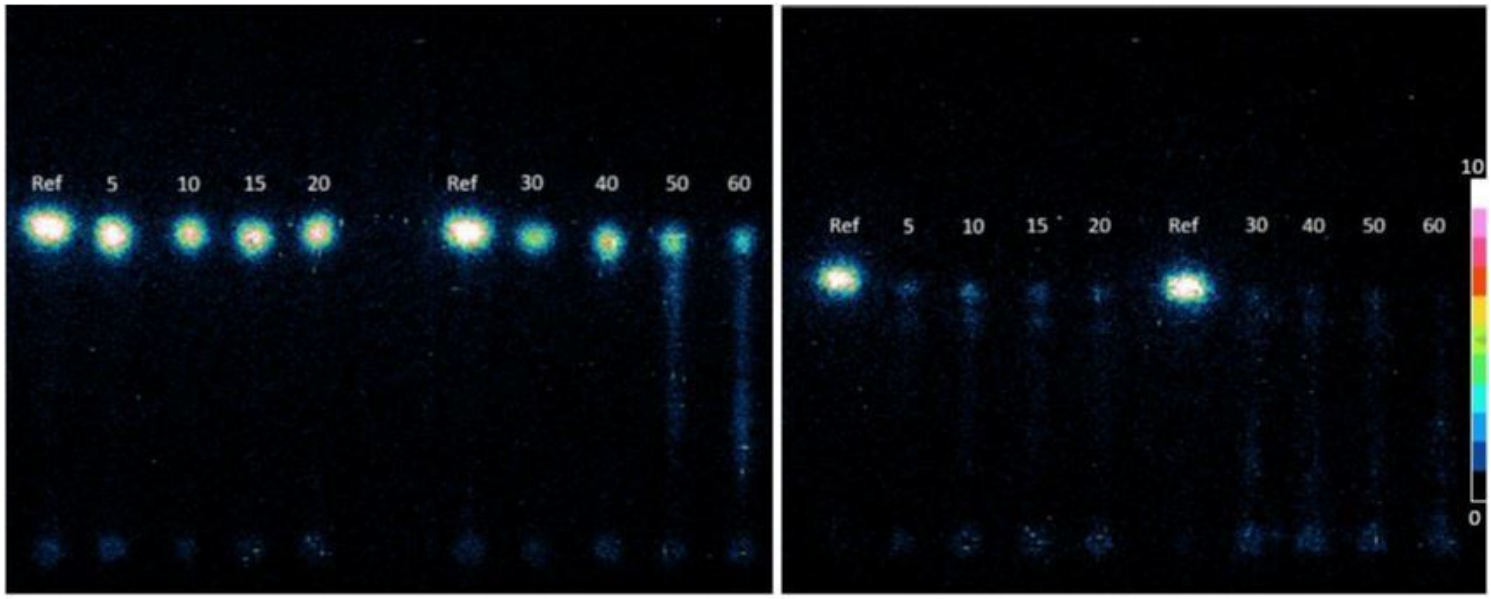

Figure 3

Autoradiographic image of plasma samples Autoradiography image of plasma samples obtained from a rat injected with [18F]FAZA (left) and from a pig injected with [18F]FEPPA (right). 'Ref' is the reference spot on each TLC plate. The number above each line shows the time in min at which the blood sample was drawn post tracer injection. The direction of motion of the mobile phase (solvent) front from capillary action was from bottom to top. The radio-metabolites that did not move with mobile phase show up as faint 'spots' at the bottom along the spotting line.

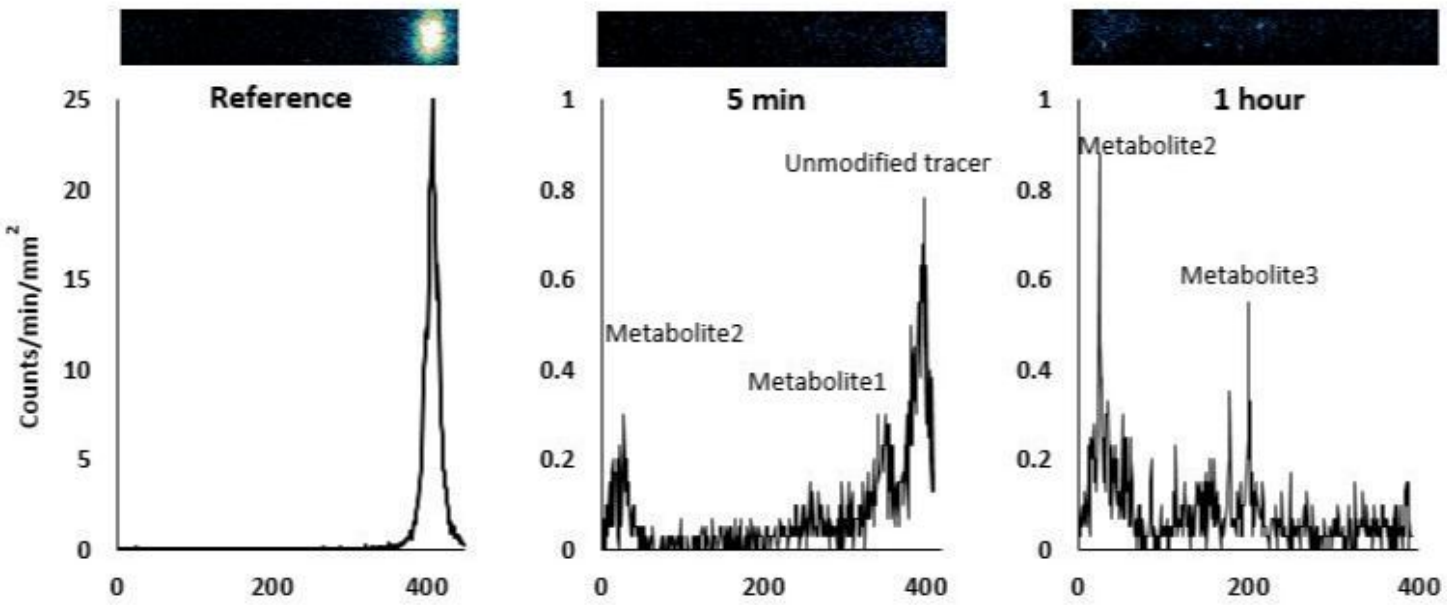

Figure 4

Line profile of [18F]FEPPA Line profile of [18F]FEPPA reference, plasma from a pig obtained at 5 min and 1 h post tracer injection. The y-axis is detected counts and the x-axis is distance in mm. The corresponding autoradiography image is displayed above the profile. The direction of movement of the solvent front from capillary action was from left to right

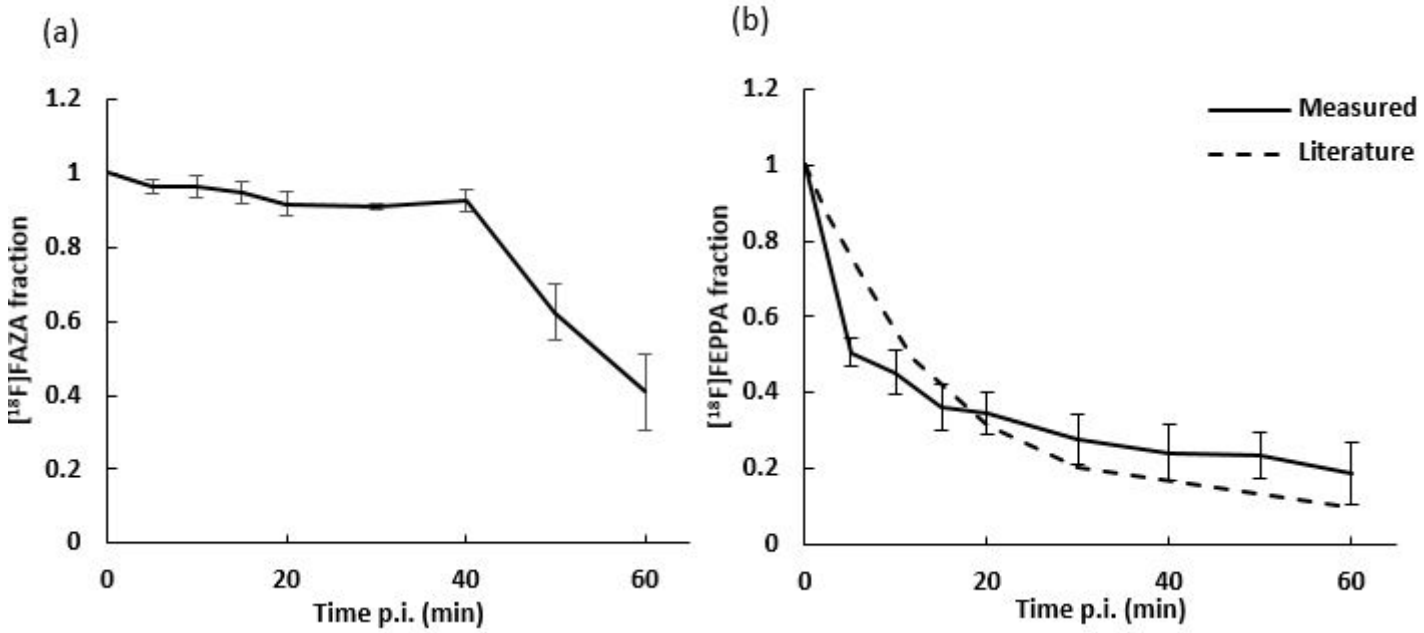

Figure 5

Fraction of parent tracer for [18F]FAZA and [18F]FEPPA Native tracer fraction vs time post injection (p.i.) for (a) [18F]FAZA and (b) [18F]FEPPA. The dashed line in (b) was native tracer fraction from (18).The error bar corresponds to standard deviation for 5 pig blood samples ([18F]FEPPA) and 4 rat blood samples ([18F]FAZA)

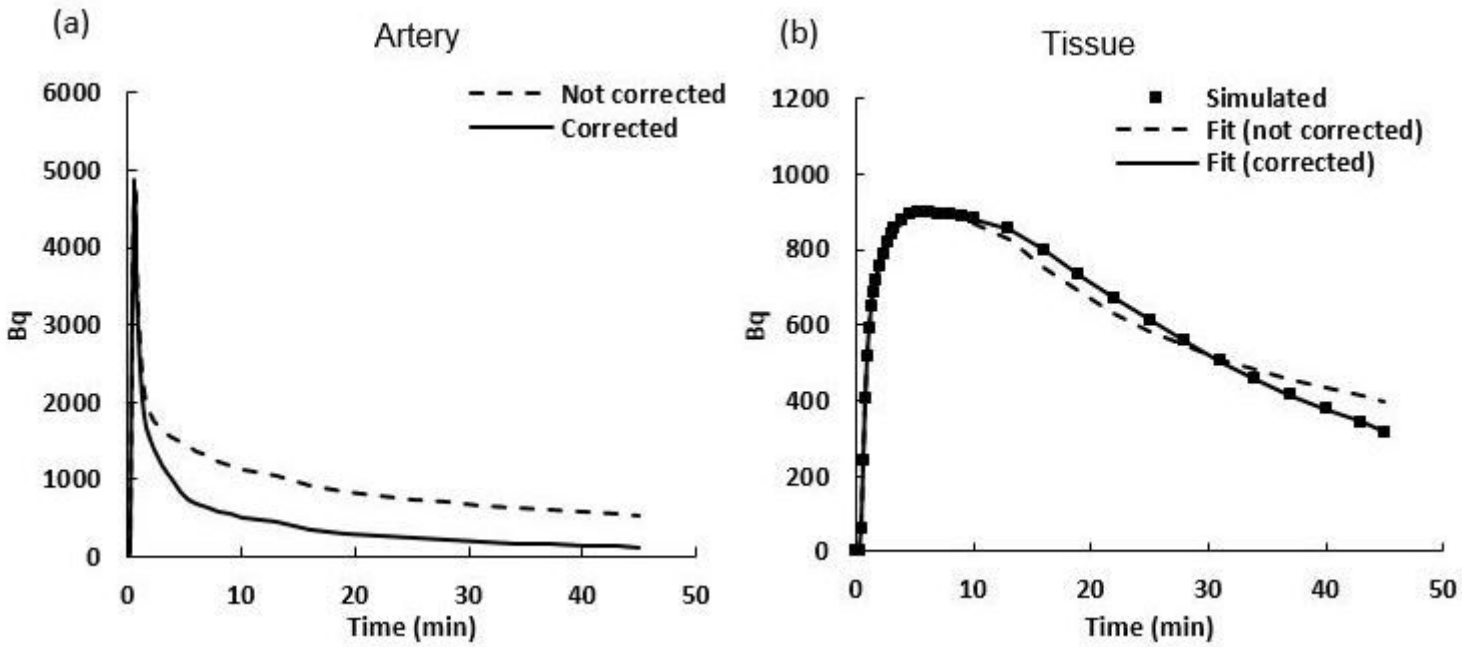

Figure 6

Simulation curves for estimating accuracy of kinetic parameter due radio-metabolite correction Curves utilized for simulating the effect of radio-metabolite on kinetic parameter estimation in dynamic PET cases. (a) Arterial curve simulated with Feng's model for measured (not corrected, dashed line) and radio-metabolite corrected curve (solid line). (b) Tissue curve simulated with parameter set #6 (table 1, solid square) and fitted curves obtained with measured arterial curve (dashed line) and with radio-metabolite corrected arterial curve (solid line).

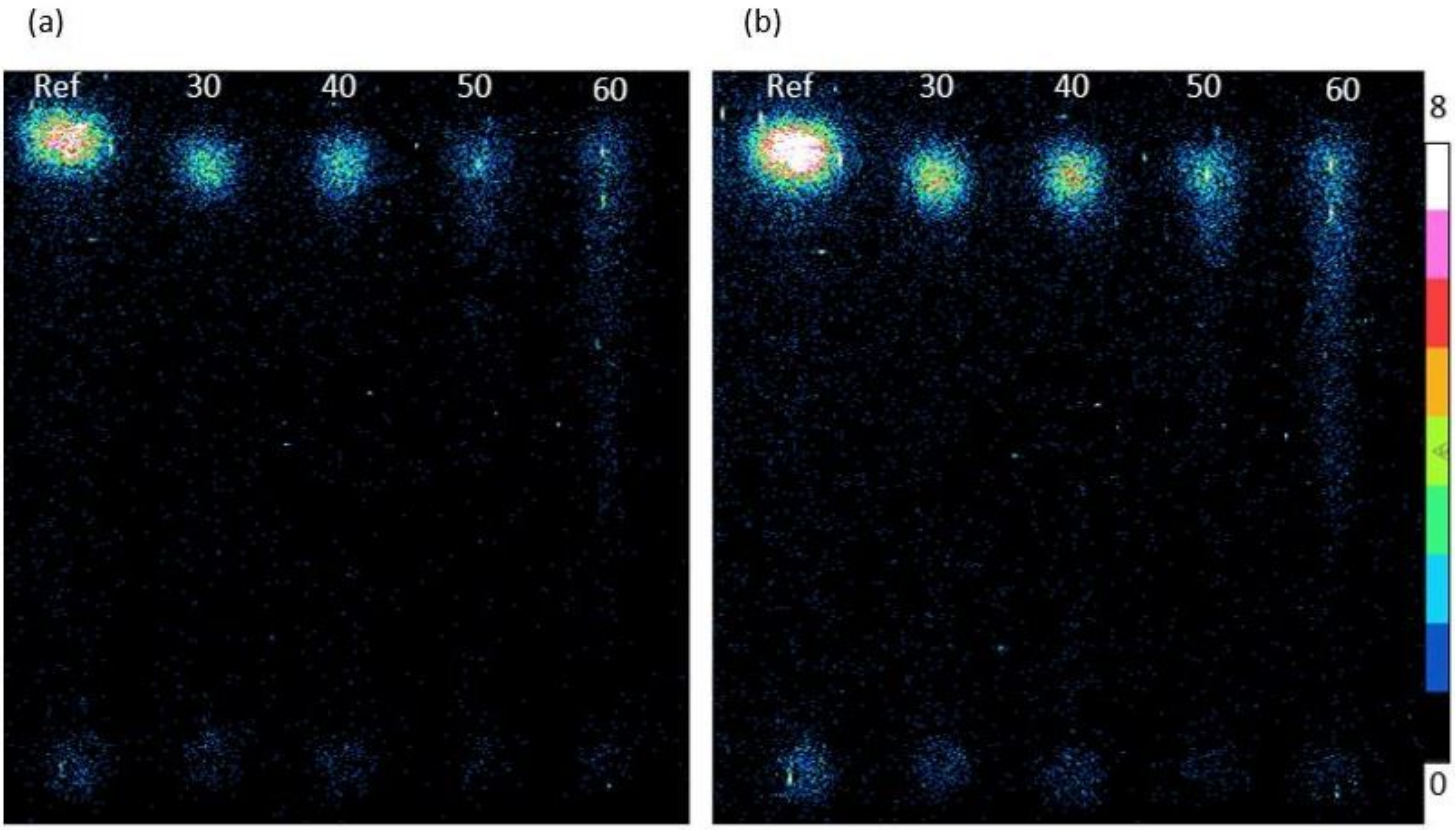

Figure 7

Beaver image of blood plasma obtained from a rat injected with [18F]FAZA. The SNR of image (a) acquire for 1 hour is acceptable with discernible spots for native tracer and radio-metabolites. (b) The same TLC image that is acquired for four hours immediately after (a) was acquired. The bright spot is the reference ‘ref’ native tracer followed by blood samples drawn at 30, 40, 50 and 60 minute post injection.

Supplementary Files

This is a list of supplementary files associated with this preprint. Click to download.

- SupplementaryFigure.tiff